

Estimation of the global solar irradiance on tilted surfaces

Marko Gulin*, Mario Vašak†, and Mato Baotic‡

University of Zagreb, Faculty of Electrical Engineering and Computing

Laboratory for Renewable Energy Systems (url: www.lares.fer.hr)

*marko.gulin@fer.hr, †mario.vasak@fer.hr, ‡mato.baotic@fer.hr

Abstract—In this paper we develop and verify 3 neural-network-based models for predicting the global solar irradiance on tilted surfaces. Models' inputs are: (i) solar irradiance components – direct (normal), diffuse (horizontal), ground reflected and/or global (horizontal) solar irradiance, (ii) sun position on the sky dome, i.e., solar zenith and azimuth angles, and (iii) tilted surface orientation angles, i.e., tilted surface tilt and azimuth angles, while models' output is the global solar irradiance incident with the tilted surface. These models are then compared with 3 isotropic and 6 anisotropic irradiance models for tilted surfaces from literature. Solar irradiance data used for model identification and verification is recorded in the 10 sec time step and then integrated on the 10 min time step through a month period in 2013, and is filtered out in order to retain only high-quality solar irradiance measurements.

Index Terms—Solar Irradiance, Tilted Surface, Ground Albedo, Isotropic Models, Anisotropic Models

I. INTRODUCTION

Importance of renewable energy sources in the world grows rapidly. Among renewable sources, solar energy is one of the most promising nowadays [1] and is predicted by numerous analyses to become the mostly used energy resource by 2050 [2]. However, photovoltaic panels (and other solar systems, e.g. solar collectors) still have weak efficiency and high cost of production, and in order to enlarge their power production gain, they are often placed in a tilted position [3]. E.g., authors in [4] use solar irradiance prediction (on a daily basis) to calculate the optimal positioning trajectory for photovoltaic panels, in order to maximize their power production considering positioning system energy consumption.

Quantitative assessment of solar irradiance incident on tilted surfaces is very important to, e.g., engineers who design advanced control and/or monitoring of power electronics converters connected to photovoltaic panels or for optimal tilt and azimuth angle positioning [4], [5]. The usage goes of course beyond photovoltaic systems and applies to different systems where input energy from sun on a tilted surface is important for system control, e.g., input solar irradiance on different outer building surfaces is very important for energy-efficient control of indoor building climate.

Meteorological stations usually measure global and diffuse solar irradiance received on horizontal surfaces. There are many models developed recently for estimation of the global solar irradiance on tilted surfaces [6], [7]. Since direct (normal) irradiance component is transformed via simple geometrical

relations [8], only difference between them is in the concept whether or not the diffuse irradiance is considered isotropically distributed over the sky dome.

In this paper we develop and verify 3 neural-network-based models for predicting the global solar irradiance on tilted surfaces for different orientation angles (i.e. tilt and azimuth angles). Models' inputs are: (i) solar irradiance components – direct (normal), diffuse (horizontal), ground reflected and/or global (horizontal) solar irradiance, (ii) sun position on the sky dome, i.e., solar zenith and azimuth angles, and (iii) tilted surface orientation angles, i.e., tilted surface tilt and azimuth angles, while models' output is the global solar irradiance incident with the tilted surface. These models are then compared with 3 isotropic [9]–[11] and 6 anisotropic [12]–[17] solar irradiance models for tilted surfaces from literature, best described in [6]. Solar irradiance data used for model identification and verification is recorded in the 10 sec time step and then integrated on the 10 min time step through a month period in 2013, and is filtered out in order to retain only high-quality solar irradiance measurements. Solar irradiance measurement station is installed on the rooftop of the skyscraper building of University of Zagreb, Faculty of Electrical Engineering and Computing (latitude: 45.80° N, longitude: 15.87° E).

This paper is organized as follows. Section II describes 3 isotropic and 6 anisotropic solar irradiance models for tilted surfaces from literature. Section III describes solar irradiance data quality control. In Section IV 3 different neural-network-based models for predicting the global solar irradiance on tilted surfaces are developed. In Section V a qualitative assessment of the developed 3 neural network models and the considered 9 models from literature is given.

II. MODELS FOR PREDICTING THE GLOBAL SOLAR RADIATION ON TILTED SURFACES

The global (or total) solar irradiance incident with a tilted surface G_φ comprises three basic components, as shown in Fig. 1: (i) direct (or beam) B_φ , (ii) sky diffuse D_φ , and (iii) reflected R_φ solar irradiance component:

$$G_\varphi = B_\varphi + D_\varphi + R_\varphi, \quad (1)$$

where vector $\varphi = [\beta, \gamma]$ represents tilted surface orientation, i.e., tilted surface tilt β and azimuth γ angles.

While measured direct (normal) irradiance is converted to direct irradiance on a tilted surface by simple geometrical relationship between the two surfaces, this is not the case for the diffuse component because diffuse irradiance comes from all points of the sky except the sun. A relatively large number of solar irradiance models for tilted surfaces have been proposed which include isotropic [9]–[11] and anisotropic [12]–[17] models.

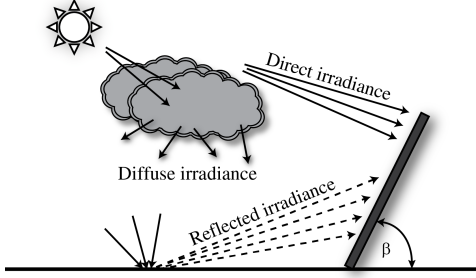


Fig. 1. Solar irradiance components.

A. Direct (tilted) irradiance, B_φ

Calculation of the direct irradiance incident with a tilted surface B_φ is purely geometrical:

$$B_\varphi = B_n \cos \theta = \frac{B_h}{\cos \theta_z} \cos \theta = B_h r_b, \quad (2)$$

where B_n and B_h are direct (normal) and direct (horizontal) solar irradiance, r_b is direct irradiance conversion factor

$$r_b = \max\left(0, \frac{\cos \theta}{\cos \theta_z}\right), \quad (3)$$

and θ is the angle of incidence, i.e., the angle between the sun direction and the normal direction of a tilted surface [8]:

$$\cos \theta = \cos \theta_z \cos \beta + \sin \theta_z \sin \beta \cos(\gamma_s - \gamma), \quad (4)$$

where θ_z and γ_s are the solar zenith and azimuth angles, respectively. Detailed angles description is shown in Fig. 2.

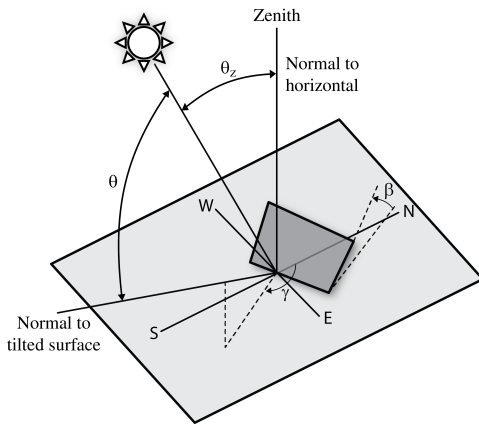


Fig. 2. Zenith angle θ_z , angle of incidence θ , tilt angle β and azimuth angle γ for a tilted surface [8].

B. Diffuse (tilted) irradiance, D_φ

Studies [18] have led to a description [6] of the diffuse component being composed of an isotropic component $D_{\varphi,iso}$ (i.e., uniform irradiance from the sky dome), circumsolar component $D_{\varphi,cs}$ (i.e., resulting from the forward scattering of solar irradiance and concentrated in an area close to the sun), and a horizon brightening component $D_{\varphi,hb}$ (i.e., concentrated in a band near the horizon and most pronounced in clear skies):

$$D_\varphi = D_{\varphi,iso} + D_{\varphi,cs} + D_{\varphi,hb}. \quad (5)$$

There are many models developed recently used to calculate diffuse solar irradiance incident with a tilted surface D_φ . Main difference between them is in the concept of whether or not the diffuse irradiance is isotropically distributed over the sky dome. In this paper we will verify 3 isotropic and 6 anisotropic models. Each model develops the diffuse transposition factor (i.e., the ratio of diffuse irradiance on a tilted surface to that of a horizontal, R_d) according to specific assumptions:

$$D_\varphi = D_h R_d, \quad R_d \geq 0, \quad (6)$$

where D_h is the diffuse (horizontal) irradiance.

ISOTROPIC MODELS

Liu-Jordan (LJ). Liu-Jordan model, [9] sets the diffuse irradiance transposition factor as:

$$R_d = \frac{1}{2}(1 + \cos \beta). \quad (7)$$

Korokanis (Ko). The isotropic sky assumption was questioned in [19] where it was found that the sky's southern part (in northern hemisphere) is responsible for 63% of the total intensity of diffuse irradiance. Based on this finding, authors in [10] modified the Liu-Jordan isotropic model as follows:

$$R_d = \frac{1}{3}(2 + \cos \beta), \quad (8)$$

for which a vertical plane oriented southwards covers 66.7% of the total sky irradiance.

Badescu (Ba). Pseudo-isotropic model proposed by authors in [11] define diffuse irradiance transposition factor as:

$$R_d = \frac{1}{4}(3 + \cos 2\beta). \quad (9)$$

ANISOTROPIC MODELS

Willmot (Wi). Authors in [12] define diffuse irradiance transposition factor as:

$$R_d = r_b \frac{B_n}{S_0} + C_\varphi \frac{S_0 - B_n}{S_0}, \quad (10)$$

where S_0 is the solar constant (i.e., 1367 Wm^{-2}), and C_φ is anisotropic reduction factor defined as:

$$C_\varphi = 1.0115 - 0.20293\beta - 0.080823\beta^2, \quad (11)$$

where the tilted surface tilt angle β is in radians.

Bugler (Bu). Authors in [13] modified the isotropic model defined in (7) by adding terms for the diffuse irradiance coming from the sun's disc and for the irradiance from the rest of the sky that depends on the angular height of the sun over the horizon:

$$R_d = R_{d,LJ} + 0.05 \frac{B_\varphi}{D_h} \left(\cos \theta - \frac{R_{d,LJ}}{\cos \theta_z} \right), \quad (12)$$

where $R_{d,LJ}$ is the Liu-Jordan isotropic model diffuse irradiance transposition factor defined in (7).

Hay (Ha). In the Hay model [14], diffuse irradiance from the sky is composed of an isotropic component and a circum-solar one. Horizon brightening is not taken into account. An anisotropy index, F_{Hay} , is used to quantify a portion of the diffuse irradiance treated as circumsolar with the remaining portion of diffuse irradiance assumed to be isotropic:

$$R_d = F_{Hay} r_b + (1 - F_{Hay}) R_{d,LJ}, \quad F_{Hay} = \frac{B_n}{G_{ext}}, \quad (13)$$

where F_{Hay} is the Hay's sky-clarity factor, and G_{ext} is the extra-atmospheric solar radiation. To simplify the model, one can use an approximation $G_{ext} = S_0$. The Hay model is reduced to the Liu-Jordan model (7) for $F_{Hay} = 0$.

Skartveit-Olseth (SO). Solar irradiance measurements indicate that a significant part of sky diffuse irradiance under overcast sky conditions comes from the sky region around the zenith. This effect vanishes when cloud cover disappears. Skartveit-Olseth [15] modified the Hay model in order to account for this effect:

$$R_d = F_{Hay} r_b + Z \cos \beta + (1 - F_{Hay} - Z) R_{d,LJ}, \quad (14)$$

where Z is the Skartveit-Olseth's correction factor defined as:

$$Z = \max(0, 0.3 - 2F_{Hay}). \quad (15)$$

Note that for $F_{Hay} \geq 0.15$, the Skartveit-Oleth's model reduces to the Hay's model.

Temps-Coulson (TC). Assuming clear sky conditions, Temps-Coulson [16] modified the Liu-Jordan isotropic model (7) by introducing two terms, P_1 and P_2 , as follows:

$$R_d = R_{d,LJ} P_1 P_2, \quad (16)$$

where term P_1 evaluate the diffuse irradiance coming from the vicinity of the solar disc, and term P_2 evaluate sky irradiance from the region close to the horizon:

$$P_1 = 1 + \cos^2 \theta \sin^3 \theta_z, \quad (17a)$$

$$P_2 = 1 + \sin^3 \frac{\beta}{2}. \quad (17b)$$

Klucher model (KI). Klucher [17] found that the isotropic model (7) gave good results for overcast skies but underestimates irradiance under clear and partly cloudy sky conditions, characterized by an increased intensity near the horizon and

near the circumsolar sky region. To overcome such a limitation, he proposed to refine Temps-Coulson model (16) by introducing a factor f_K determining the degree of cloud cover:

$$R_d = R_{d,LJ} (1 + f_K \cos^2 \theta \sin^3 \theta_z) (1 + f_K \sin^3 \frac{\beta}{2}), \quad (18)$$

where f_K is the Kluchers' conversion factor defined as:

$$f_K = 1 - \left(\frac{D_h}{G_h} \right)^2, \quad (19)$$

where G_h is global (horizontal) solar irradiance defined as:

$$G_h = B_n \cos \theta_z + D_h. \quad (20)$$

Note that for $f_K = 0$ (i.e. during the clear sky conditions) and $f_K = 1$ (i.e. during the overcast conditions), Klucher's model reduces to the Liu-Jordan model and the Temps-Coulson model, respectively.

C. Reflected (tilted) irradiance, R_φ

The classical approach to the modelling of the reflected irradiance assumes that reflected rays are diffuse and coefficients of reflection of the direct and diffuse rays are identical. The evaluation of the ground reflected diffuse irradiance R_φ is thus dependent on the transposition factor for ground reflection R_h :

$$R_\varphi = \rho G_h R_h, \quad (21)$$

where ρ is the foreground's albedo. Most studies assume [6] that a constant irradiance originates from every point of the ground, i.e. the ground reflection process is ideally isotropic. In this case, transposition factor for ground reflection can be simplified into:

$$R_h = \frac{1}{2} (1 - \cos \beta). \quad (22)$$

III. IRRADIANCE DATA QUALITY CONTROL

The presented analysis is based upon measurements recorded at the rooftop of the skyscraper building of University of Zagreb, Faculty of Electrical Engineering and Computing (latitude: 45.80° N, longitude: 15.97° E). Eight data sets have been collected through a month period in 2013: (i-iv) direct (normal) B_n , diffuse (horizontal) D_h , ground reflected R_g , and global (horizontal) G_h solar irradiance, and (v-viii) global solar irradiance incident with a south-oriented tilted surface G_φ at following tilt angles β : 5°, 30°, 55°, and 80°. The irradiance measurements are recorded with a time step of 10 sec and then integrated on a 10 min time step.

The direct (normal) irradiance is measured with a first class CHP 1 sun tracker pyrhelimeter with additional sun sensor for closed-loop sun tracking, while the diffuse (horizontal), ground reflected, and global (horizontal) irradiance are measured with CMP 11 – secondary standard pyranometers. Global solar irradiance incident with a tilted surface is measured with CMP 6 pyranometers. For the diffuse measurements, a shading ball is mounted in front of the pyranometer with same solid angle as the pyrhelimeter blocking out the direct component.



Fig. 3. SOLYS2 sun tracker with solar irradiance measurement equipment and sun tracker for closed-loop sun tracking

In order to retain only high-quality irradiance measurement for identification and verification, irradiance data are filtered out with the following criteria:

$$0.95G_{h,\text{meas}} \leq G_{h,\text{est}} \leq 1.05G_{h,\text{meas}}, \quad (23)$$

where $G_{h,\text{meas}}$ and $G_{h,\text{est}}$ are measured and estimated (20) global (horizontal) solar irradiance. Approximately 98.9% of solar irradiance data samples recorded meet condition (23) (considering only sunshine hours, i.e., $\theta_z < 90^\circ$).

IV. DEVELOPMENT OF THE NEURAL NETWORK MODEL

Used neural network structure is MultiLayer Perceptron (MLP) neural network [20], [21] with one hidden and output layer. Neural network is a mathematical function with a number of parameters that are fitted in a way so that difference between target y_t and neural network output y_{MLP} is minimized for the given set of input-target pairs for training. Cost-function used for neural network training (parameters tuning by cost-function minimization) is Mean Square Error (MSE):

$$\text{MSE} = \frac{1}{N} \sum_{s=1}^N e_s^2, \quad e_s = y_{t,s} - f_{\text{MLP}}(\mathbf{X}_s, \boldsymbol{\theta}), \quad (24)$$

where N is number of input-target measurement pairs, e is neural network model error, $(\mathbf{X}_s, y_{t,s})$ is s -th input-target pair, $f_{\text{MLP}}(\cdot, \cdot)$ is mathematical function that describes used MLP neural network, and $\boldsymbol{\theta}$ is vector of neural network parameters.

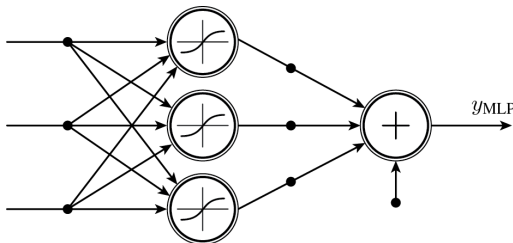


Fig. 4. MLP neural network structure with tansig function in hidden layer

Neural network models inputs are: (i-iv) solar irradiance components – direct (normal), diffuse (horizontal), ground reflected and/or global (horizontal) solar irradiance, (v-vi) sun position on the sky dome, i.e., solar zenith and azimuth angles, and (vii-viii) tilted surface orientation angles, i.e., tilted surface tilt and azimuth angles, while models' output is the global solar irradiance incident with the tilted surface. Three different neural network models are considered, denoted as: (i) full-input (MLP-F), (ii) full-input hybrid (MLP-H), and (iii) reduced-input (MLP-R) neural network. Full-input neural networks do not use global (horizontal) solar irradiance data as inputs, while reduced-input neural network does not use direct (normal) and ground reflected solar irradiance since those components are most likely not available by meteorological service. Hybrid neural network additionally takes into account transformation of direct (normal) to direct (tilted) solar irradiance, so that target vector of hybrid neural network is:

$$y_{t,\text{MLP-H}} = G_\delta - B_\delta, \quad (25)$$

where G_δ is measured global solar irradiance incident with a tilted surface, and B_δ is transformed direct (normal) to direct (tilted) solar irradiance (see Eq. (2)) at orientation angle δ . In this way, hybrid neural network model practically identifies transformation of only diffuse (horizontal) and ground reflected solar irradiance components.

There are several properties that need to be defined by the user before neural network training can begin. Those are primarily: (i) neural network training method, (ii) neural network training stop criteria to prevent overfitting, and (iii) neural network complexity (determined by number of hidden layers, and by number of neurons, i.e., nonlinear activation functions in each hidden layer).

Neural network training refers to parameters tuning considering some cost-function. Training will continue until stopping criteria are satisfied (e.g., maximum number of iterations and/or elapsed time). However, to prevent overfitting wherein neural network can learn even noise, aforementioned stopping criteria are not enough. To prevent overfitting, data set is divided on training and validation data sets, with shares of 70% and 30% of whole data set, respectively. Neural network parameters tuning is done considering only training data set, but cost-function is also calculated for validation data set. When cost-function (considering only validation data set) shows no improvement through some predefined number of iterations (e.g., 10 iterations), training is stopped and best performing parameters vector considering validation data set is used. For neural network training (i.e. parameters tuning), a gradient-based Levenberg-Marquardt algorithm is used.

One must have in mind that too simple neural network (small number of neurons) might not be able to perform well, while too complex network (large number of neurons) can be too demanding for training algorithm. Also, complexity of neural network increases exponentially with number of hidden layers. In most fitting practical problems, one hidden layer with 15-20 neurons is enough for neural network to perform well. Neural network training procedure (for each of

the considered 3 neural network models) is done with different numbers of neurons (8 different sizes uniformly distributed from 5 to 40 neurons), and is repeated 100 times for each mode, which gives $3 \times 8 \times 100 = 2400$ neural network trainings in total. Mean, worst and best cost-function value through 100 trainings (on validation data set) for each model and hidden layer size is shown in Fig. 24. It is shown that optimal hidden layer size is 15–20 neurons, and that with increasing number of neurons, neural network performance can be even worse. It is also shown that for small number of neurons, hybrid model shows far best performance compared to other two neural network models. This is in line with expectation, since hybrid model does not have to learn transformation of direct (normal) to direct (tilted) irradiance.

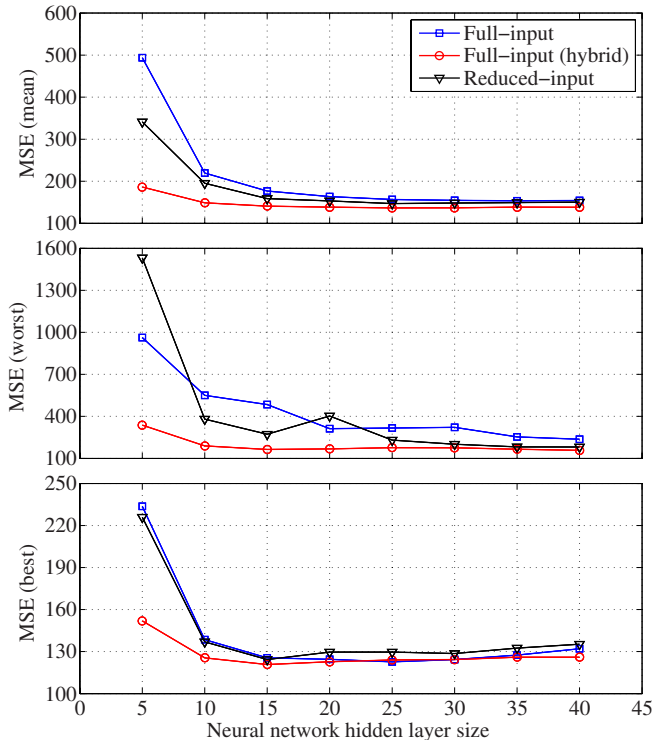


Fig. 5. Mean, worst and best cost-function value in W^2/m^4 through 100 trainings for 3 different models and 8 different hidden layer sizes.

V. QUALITATIVE ASSESMENT OF THE DEVELOPED 3 AND THE CONSIDERED 9 MODELS

Performance measures used for models verification are Mean Bias Error (MBE), Mean Square Error (MSE), and Root Mean Square Error (RMSE), defined as:

$$MBE = \frac{1}{N} \sum_{s=1}^N e_s, \quad RMSE = \sqrt{\frac{1}{N} \sum_{s=1}^N e_s^2}. \quad (26)$$

Besides MBE, MSE and RMSE, a linear regression R (i.e. correlation coefficient) is also used to test models' performance. Table I shows performance indicators, and Fig. 6 shows regression plots of developed 3 best performing neural

network models and considered 9 models. Verification of developed neural network models is done only on validation data set, while verification of considered 9 models is done on whole data set. It is shown that developed neural network models significantly outperform considered 9 models by all performance indicators. However, downside of this approach is that neural network models are applicable only for the measurement test site.

Similar performance results for considered 9 models shown in Table I are also given in [6]. Nevertheless, we obtained somewhat better performance indicators, mainly because of more quality measurements of solar irradiance components and fewer measurement days considered in the data set. Developed neural network models will help us make a new non-site-specific model once a more larger measurement days data set is collected, as they showed that there exists a nonlinearity that considered 9 models did not take into account.

TABLE I
PERFORMANCE INDICATORS OF CONSIDERED MODELS

	MBE (W/m^2)	MSE (W^2/m^4)	RMSE (W/m^2)	R
MLP-F	0.09	122.64	11.07	0.99932
MLP-H	-0.43	121.06	11.00	0.99933
MLP-R	0.49	124.32	11.15	0.99931
LJ	4.71	436.03	20.88	0.99817
Ko	-4.84	619.55	24.89	0.99706
Ba	15.17	798.56	28.26	0.99760
Wi	8.86	503.85	22.45	0.99782
Bu	10.09	578.12	24.04	0.99804
Ha	4.26	393.23	19.83	0.99812
SO	6.85	428.92	20.71	0.99802
TC	-17.82	977.66	31.27	0.99648
KI	-9.32	531.90	23.06	0.99763

VI. CONCLUSION

In this paper we developed and verified 3 different neural network models for prediction of solar irradiance incident with a tilted surface. Performance of the developed neural network models is compared to performance of most competitive 3 isotropic and 6 anisotropic models for tilted surface from literature. It is shown that neural network models significantly outperform the considered 9 models. However, downside of this approach is that developed models are applicable only for the measurement test site. Developed neural network models will help us make a new non-site-specific model once a more larger measurement days data set is collected.

ACKNOWLEDGMENT

This work has been financially supported by the European Union through project ENHEMS-Buildings – Enhancement of Research, Development and Technology Transfer Capacities in Energy Management Systems for Buildings under grant No. IPA2007/HR/16IPO/001-040510, and by the Croatian Science Foundation under grant No. I-4463-2011 (MICROGRID). This support is gratefully acknowledged.

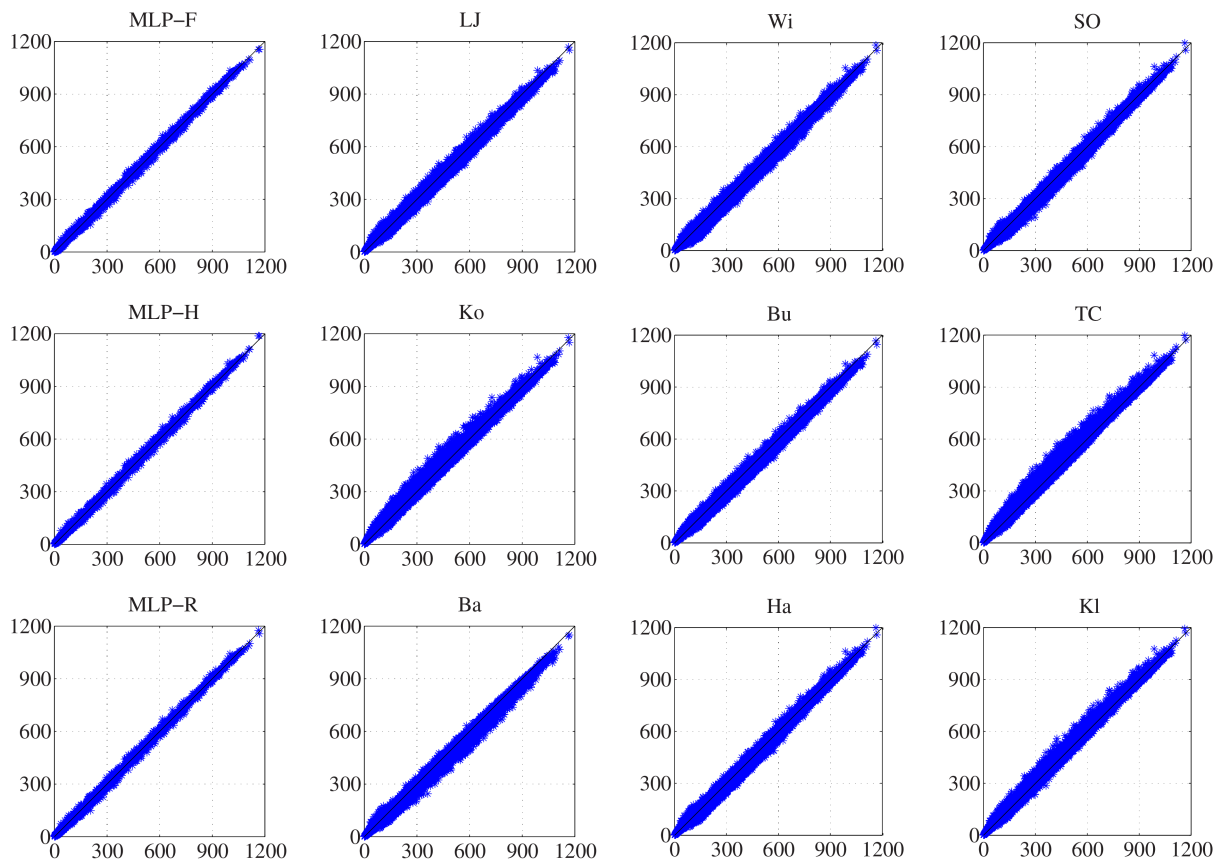


Fig. 6. Regression plots of 3 developed neural network models and considered 3 isotropic and 6 anisotropic models for predicting global solar irradiance on tilted surfaces. Horizontal axis shows measured solar irradiance (W/m^2), while vertical axis shows estimated solar irradiance (W/m^2) on tilted surface.

REFERENCES

- [1] J. L. Sawin, "Renewables 2013: Global Status Report," REN21 Secretariat, 2013.
- [2] "World in Transition: A Social Contract for Sustainability," German Advisory Council on Global Change, 2011.
- [3] J. Kaldellis, K. Kavadias, and D. Zafirakis, "Experimental validation of the optimum photovoltaic panels' tilt angle for remote consumers," *Renewable Energy*, vol. 46, no. 0, pp. 179–191, October 2012.
- [4] M. Gulin, M. Vařak, and N. Perić, "Dynamical optimal positioning of a photovoltaic panel in all weather conditions," *Applied Energy*, vol. 108, no. 0, pp. 429–438, August 2013.
- [5] E. D. Mehleri, P. L. Zervas, H. Sarimveis, J. A. Palyvos, and N. C. Markatos, "Determination of the optimal tilt angle and orientation for solar photovoltaic arrays," *Renewable Energy*, vol. 35, no. 11, pp. 2468–2475, November 2010.
- [6] C. Demain, M. Journée, and C. Bertrand, "Evaluation of different models to estimate the global solar radiation on inclined surfaces," *Renewable Energy*, vol. 50, no. 0, pp. 710–721, February 2013.
- [7] M. David, P. Lauret, and J. Boland, "Evaluating tilted plane models for solar radiation using comprehensive testing procedures, at a southern hemisphere location," *Renewable Energy*, vol. 51, no. 0, pp. 124–131, March 2013.
- [8] J. Twidell and T. Weir, *Renewable Energy Resources*, 2nd ed. Taylor & Francis, 2005.
- [9] B. Y. H. Liu and R. C. Jordan, "Daily insolation on surfaces tilted towards the equator," *ASHRAE Journal*, vol. 3, no. 0, pp. 53–59, 1961.
- [10] P. S. Koronakis, "On the choice of the angle of tilt for south facing solar collectors in the athens basin area," *Solar Energy*, vol. 36, no. 3, pp. 217–225, 1986.
- [11] V. Badescu, "3D isotropic approximation for solar diffuse irradiance on tilted surfaces," *Renewable Energy*, vol. 26, no. 2, pp. 221–233, June 2002.
- [12] C. J. Willmott, "On the climatic optimization of the tilt and azimuth of flat-plate solar collectors," *Solar Energy*, vol. 28, no. 3, pp. 205–216, 1982.
- [13] J. W. Bugler, "The determination of hourly insolation on an inclined plane using a diffuse irradiance model based on hourly measured global horizontal insolation," *Solar Energy*, vol. 19, no. 5, pp. 477–491, 1977.
- [14] J. E. Hay, "Calculation of monthly mean solar radiation for horizontal and inclined surfaces," *Solar Energy*, vol. 23, no. 4, pp. 301–307, 1979.
- [15] A. Skartveit and J. A. Olseth, "Modelling slope irradiance at high latitudes," *Solar Energy*, vol. 36, no. 4, pp. 333–344, 1986.
- [16] R. C. Temps and K. L. Coulson, "Solar radiation incident upon slopes of different orientations," *Solar Energy*, vol. 19, no. 2, pp. 179–184, 1977.
- [17] T. M. Klucher, "Evaluation of models to predict insolation on tilted surfaces," *Solar Energy*, vol. 23, no. 2, pp. 111–114, 1979.
- [18] R. Perez, R. Stewart, C. Arbogast, R. Seals, and J. Scott, "An anisotropic hourly diffuse radiation model for sloping surfaces: Description, performance validation, site dependency evaluation," *Solar Energy*, vol. 36, no. 6, pp. 481–497, 1986.
- [19] H. L. Hamilton and A. Jackson, "A shield for obtaining diffuse sky radiation from portions of the sky," *Solar Energy*, vol. 34, no. 1, pp. 121–123, 1985.
- [20] S. Haykin, Ed., *Kalman Filtering and Neural Networks*, 1st ed. Wiley-Interscience, 2001.
- [21] M. S. Grewal and A. P. Andrews, *Kalman Filtering: Theory and Practice Using MATLAB*, 3rd ed. Wiley-IEEE Press, 2008.